Confinement of excitons in quantum dots

G.T. Einevoll*

Institutt for Fysikk, Norges Tekniske Høgskole, Universitetet i Trondheim, N-7034 Trondheim, Norway

(Received 25 June 1991)

A theoretical study of exciton confinement in small CdS and ZnS quantum dots is reported. In our calculational scheme the hole is described by an effective bond-orbital model that accounts for the valence-band degeneracy in bulk semiconductors. The electron is described with a single-band effective-mass approximation. The confining quantum-dot potentials for the hole and electron are modeled as spherically symmetric potential wells with finite barrier heights. The electron-hole Coulomb attraction is included and exciton energies are obtained variationally in an iterative Hartree scheme. Exciton energies for dot diameters in the range 10–80 Å are calculated and compared with experimental data and other theoretical results.

I. INTRODUCTION

Effects of quantum confinement of excitons in semiconductor crystallites have been extensively investigated in recent years.[1-8] As the size of the crystallite, or, alternatively, the quantum dot, becomes smaller and approaches the Bohr radius of the bulk exciton, quantum-confinement effects become apparent, and a blue-shift in the exciton energy can be observed. Experimentally a wide variety of systems have been studied.[9] In particular, small crystallites of CdS and ZnS with diameters between 10 and 60 Å have been produced and studied.[2,6,10,11] Surprisingly, they generally exhibit the same zinc-blende structure as in bulk (except possibly the smallest crystallites.[6]) Optical-absorbtion spectra have revealed that exciton energies are blue-shifted compared to the value in bulk, and this has been explained in terms of quantum confinement of the exciton.

On the theoretical side most studies have been based on the effective-mass approximation.[1,3,8,12,13] In these calculations both electron and hole have been described with single-band effective-mass theories with spherical effective masses. The attractive Couloumb interaction has been included in addition to spherically symmetric confining potentials due to the (spherical) quantum dot. With only one exception,[8] the confining potentials for the electron and the hole have been assumed infinite outside the quantum dot, i.e., hard walls. The effective-mass equation has been solved variationally with different choices of trial wave functions. There are two limiting cases depending upon the ratio between the radius of the quantum dot R and the effective Bohr radius of the bulk exciton a^*. For $R/a^* \gg 1$ the exciton can be envisioned as a quasiparticle moving around inside the quantum dot with only little energy increment due to confinement. In the opposite limit, $R/a^* \ll 1$, confinement effects dominate, and the electron and hole should be viewed as individual particles predominantly in their respective single-particle ground states with only little spatial correlation between them. In this regime, called the strong-confinement regime, Kayanuma found the follow-

ing approximate expression for the confinement energy:[3]

$$E = \frac{\hbar^2}{2}\left(\frac{1}{m_e} + \frac{1}{m_h}\right)\frac{\pi^2}{R^2} - 1.786\frac{e^2}{\epsilon R} - 0.248 E^*_{Ry}\ .$$

$$(1)$$

Here m_e and m_h are the electron and hole effective masses, respectively, and ϵ is the dielectric constant. The effective Rydberg (in meV) is defined as

$$E^*_{Ry} = 13605.8\frac{1}{\epsilon^2}\left(\frac{m_0}{m_e} + \frac{m_0}{m_h}\right)^{-1}\ ,$$

$$(2)$$

where m_0 is the free-electron mass. The first term in (1) corresponds to the sum of the single-particle ground-state energies, the second term to the Coulomb attraction, and the third term to spatial correlations between the two particles. Defining the strong-confinement regime by the absence of substantial electron-hole correlations, Kayanuma found that this is not limited to $R/a^* \ll 1$, but remains valid up to about $R = 2a^*$.

The approximation of assuming an infinite potential in the surrounding medium, called the *barrier* material, in which the quantum dots are embedded, must break down for sufficiently small dot sizes. In realistic systems the wave function will penetrate into the barrier, and, in the zero-radius limit, the exciton energy will approach the bulk value in the barrier material. To account for experimental data for the smallest crystallites, finite barrier heights must be incorporated in the model. In a very recent study Kayanuma[8] included this in the effective-mass Hamiltonian and found the effect of leakage of the wave function outside the quantum dot to be substantial for experimentally relevant CdS crystallites.

Lippens and Lannoo[4] used a tight-binding approach to study the *single-particle* electron and hole energies for small CdS and ZnS crystallites. Their scheme corresponds to infinite barrier heights. In their largest calculation 2500 atoms were included in a spherically shaped cluster with a radius of ~ 25 Å. Compared to effective-mass results (with infinite barrier heights) they generally

found smaller shifts in energy due to confinement.

In the present study we calculate exciton energies for small quantum dots, i.e., dots in the strong-confinement regime. We go beyond the single-band effective-mass approximation for holes by describing them within the formalism of the effective bond-orbital model (EBOM).[14] Since the bulk valence bands are degenerate at the zone center, a single-band effective-mass approach is in general not able to give a quantitatively accurate description. In fact four parameters, the three Luttinger parameters γ_1, γ_2, and γ_3 (Ref. 15) and the spin-orbit splitting Δ are needed to describe the valence bands close to their tops. In previous calculations the use of the single-band theory has been motivated only by the formidable technical simplifications in the calculational scheme, and no justification has been given. In the EBOM, which is a tight-binding-like model, the interaction parameters are fitted to the experimentally observed bulk band structure around the valence-band maxima. The model can thus be viewed as a discretized version of the multi-band effective-mass approximation[16] (with the grid given by the lattice constant). In our scheme the electron is described with the single-band effective-mass approximation. Finite barrier heights, both for the electron and the hole, are accounted for in the model. The Coulomb attraction is included, and a variational iterative Hartree scheme is pursued to calculate exciton energies.

In Sec. II the calculational method is outlined. In Sec. III we compare the EBOM results with results from a single-band effective-mass description and a tight-binding description of a single hole for a test case (spherical ZnS quantum dots with hard walls at the dot boundary). In Sec. IV we calculate energies of excitons in spherical CdS quantum dots with radii between 6 and 40 Å, for a set of different barrier heights. Our results are compared with experimental data and previous theoretical results. A calculation on an experimental relevant ZnS system is also reported. A brief conclusion is given in Sec. V.

II. CALCULATIONAL METHOD

Recently, a study of excitons bound to isoelectronic impurities in bulk ZnSe and in $ZnSe-Zn_{1-x}Mn_xSe$ strained quantum wells was reported.[17] The calculational scheme used there resembles the scheme pursued in the present exciton study. Thus in the description below some of the methical details are omitted or only briefly outlined.

For a more complete account of the method we refer to Ref. 17.

The model Hamiltonian we use to describe the exciton localized in a quantum dot is

$$H = H_h(\nabla_h, \mathbf{r}_h) + H_e(\nabla_e, \mathbf{r}_e) + v(|\mathbf{r}_h - \mathbf{r}_e|) , \quad (3)$$

where H_h (H_e) is the Hamiltonian for a hole (electron) seeing the quantum-dot potential only, and $v(|\mathbf{r}_h - \mathbf{r}_e|)$ accounts for the attractive Coulomb interaction between electron and hole. The exciton energy E is found by minimizing

$$< \Psi(\mathbf{r}_e, \mathbf{r}_h)|H|\Psi(\mathbf{r}_e, \mathbf{r}_h) >= E < \Psi(\mathbf{r}_e, \mathbf{r}_h)|\Psi(\mathbf{r}_e, \mathbf{r}_h) > \quad (4)$$

in a self-consistent Hartree scheme. The two-particle wave function is assumed separable, i.e. $\Psi(\mathbf{r}_e, \mathbf{r}_h) = \psi_e(\mathbf{r}_e)\psi_h(\mathbf{r}_h)$. Since we are in the strong-confinement regime where correlation effects are relatively small, this should be a good approximation. The separable form of the wave function naturally splits (4) into two parts, a hole part and an electron part, which are coupled via a Coulomb term. The hole and electron parts are treated consecutively, by solving a secular equation for a given set of basis functions, with the wave function from the previous solution used as input. Typically four or five iterations are needed to obtain the desired accuracy.

Both CdS and ZnS are large-gap semiconductors [$E_g \simeq$ 2.5 eV for CdS and $E_g \simeq 3.7$ eV for ZnS (Ref. 4)], and for the kinetic part of the Hamiltonian the electron and hole can be assumed decoupled.[18] We use a version of EBOM which includes six spin-orbit-coupled bond orbitals (SOBO's) to describe holes in ZnS and (cubic) CdS. This corresponds to a multiband effective-mass description which incorporates the heavy-hole, light-hole, and split-off valence bands. The hole description presented below is valid for systems with quantum-well symmetry even though the present system has the larger cubic symmetry as in bulk systems. As in Ref. 17 we use the notation for the point-group D_{2d} corresponding to quantum-well symmetry.

In D_{2d} the p-like valence orbitals transform according to the Γ_4 and Γ_5 representations, while the electron spin ($s = \frac{1}{2}$) transforms as Γ_6. According to group theory $(\Gamma_4 + \Gamma_5) \times \Gamma_6 = \Gamma_6 + {}^1\Gamma_7 + {}^2\Gamma_7$. The p-like bond orbitals and the electron spin thus combine to a Γ_6-like and two different Γ_7-like pairs of SOBO's. These are[19]

$$|\mathbf{R}, u_{\frac{1}{2}}^{\Gamma_6} >= \frac{i}{\sqrt{2}}|\mathbf{R}, x > \phi_{-\frac{1}{2}}^{\Gamma_6} + \frac{1}{\sqrt{2}}|\mathbf{R}, y > \phi_{-\frac{1}{2}}^{\Gamma_6} , \quad (5)$$

$$|\mathbf{R}, u_{-\frac{1}{2}}^{\Gamma_6} >= \frac{i}{\sqrt{2}}|\mathbf{R}, x > \phi_{\frac{1}{2}}^{\Gamma_6} - \frac{1}{\sqrt{2}}|\mathbf{R}, y > \phi_{\frac{1}{2}}^{\Gamma_6} , \quad (6)$$

$$|\mathbf{R}, {}^1 u_{\frac{1}{2}}^{\Gamma_7} >= -\frac{i}{\sqrt{6}}|\mathbf{R}, x > \phi_{-\frac{1}{2}}^{\Gamma_6} + \frac{1}{\sqrt{6}}|\mathbf{R}, y > \phi_{-\frac{1}{2}}^{\Gamma_6} + i\frac{2}{\sqrt{6}}|\mathbf{R}, z > \phi_{\frac{1}{2}}^{\Gamma_6} , \quad (7)$$

$$|\mathbf{R}, {}^1 u_{-\frac{1}{2}}^{\Gamma_7} >= \frac{i}{\sqrt{6}}|\mathbf{R}, x > \phi_{\frac{1}{2}}^{\Gamma_6} + \frac{1}{\sqrt{6}}|\mathbf{R}, y > \phi_{\frac{1}{2}}^{\Gamma_6} + i\frac{2}{\sqrt{6}}|\mathbf{R}, z > \phi_{-\frac{1}{2}}^{\Gamma_6} , \quad (8)$$

$$|\mathbf{R},^2 u_{\frac{1}{2}}^{\Gamma_7} >= -\frac{i}{\sqrt{3}}|\mathbf{R}, x > \phi_{-\frac{1}{2}}^{\Gamma_6} + \frac{1}{\sqrt{3}}|\mathbf{R}, y > \phi_{-\frac{1}{2}}^{\Gamma_6} - \frac{i}{\sqrt{3}}|\mathbf{R}, z > \phi_{\frac{1}{2}}^{\Gamma_6} , \tag{9}$$

$$|\mathbf{R},^2 u_{-\frac{1}{2}}^{\Gamma_7} >= -\frac{i}{\sqrt{3}}|\mathbf{R}, x > \phi_{\frac{1}{2}}^{\Gamma_6} - \frac{1}{\sqrt{3}}|\mathbf{R}, y > \phi_{\frac{1}{2}}^{\Gamma_6} + \frac{i}{\sqrt{3}}|\mathbf{R}, z > \phi_{-\frac{1}{2}}^{\Gamma_6} . \tag{10}$$

Here ϕ^{Γ_6} denotes the electron spinor and $|\mathbf{R}, \alpha >$ denotes an α-like ($\alpha = x, y, z$) bond orbital located at a site $\mathbf{R}$ in the face-centered-cubic lattice. The bond orbitals are assumed orthonormal, i.e., $< \mathbf{R}', \alpha'|\mathbf{R}, \alpha >= \delta_{R,R'}\delta_{\alpha,\alpha'}$, and only on-site and nearest-neighbor interactions are taken into account. The general form of these interactions are[14]

$$< \mathbf{R}, \alpha| H |\mathbf{R}', \alpha' >= E_p \delta_{R,R'}\delta_{\alpha,\alpha'}$$
$$+ \sum_\tau \delta_{R'-R,\tau}\{E_{xy}\tau_\alpha\tau_{\alpha'}(1 - \delta_{\alpha,\alpha'}) + [E_{xx}\tau_\alpha^2 + E_{zz}(1 - \tau_\alpha^2)]\delta_{\alpha,\alpha'}\} \tag{11}$$

where $E_{\alpha,\alpha'}$ is the interaction between an α-like orbital and an α'-like orbital located at the origin and at $(1,1,0)a/2$, respectively. E_p, E_{xx}, E_{xy}, and E_{zz} are four independent interaction parameters, and the sum over τ covers the 12 nearest-neighbor position vectors. τ_α denotes the α component of τ in units of $a/2$. The independent interaction parameters are determined by expanding the tight-binding Hamiltonian, $H(\mathbf{k})$, based on Eq.(11), to second order in $\mathbf{k}$ and requiring equivalence with multiband effective-mass theory. This scheme is thoroughly discussed in Ref. 14, and we merely quote the results. In terms of the Luttinger parameters γ_1, γ_2, and γ_3 the interaction parameters are found to be

$$E_{xy} = 6\gamma_3 R_0 ,$$

$$E_{xx} = (\gamma_1 + 4\gamma_2)R_0 ,$$

$$E_{zz} = (\gamma_1 - 8\gamma_2)R_0 , \tag{12}$$

$$E_p = E_v - 12\gamma_1 R_0 .$$

Here $R_0 \equiv \hbar^2/(2m_0 a^2)$ and E_v denotes the band edge of the heavy-hole and light-hole valence bands. The interactions in (12) apply for electronlike SOBO's. For convenience we use the hole picture in the following and use hole-like SOBO's for which the interactions in (12) must be multiplied with -1.

The spin-orbit coupling, which is not included in (11), lifts the energies of the SOBO's in (9) and (10) with an energy Δ, the spin-orbit splitting, compared to the other SOBO's,[16] i.e.,

$$< \mathbf{R}', u_{m'}^{\Gamma_6}|V_{so}|\mathbf{R}, u_m^{\Gamma_6} >$$

$$=< \mathbf{R}',^1 u_{m'}^{\Gamma_7}|V_{so}|\mathbf{R},^1 u_m^{\Gamma_7} >= 0 , \tag{13}$$

$$< \mathbf{R}',^2 u_{m'}^{\Gamma_7}|V_{so}|\mathbf{R},^2 u_m^{\Gamma_7} >= \Delta\, \delta_{R,R'}\delta_{m,m'} .$$

The interaction energies between bond orbitals are given in terms of the Luttinger parameters, the spin-orbit splitting Δ, and the energy of the heavy-hole and light-hole valence-band edge. For simplicity we assume the barrier material to have zinc-blende structure and

the same Luttinger parameters and spin-orbit splitting as the well material. Although this is certainly not so in realistic systems, the error introduced should not be too severe for large confining potentials, since for finite, but high, barriers the wave functions barely penetrate into the barrier material. The confining quantum-dot potential for the hole, denoted V_h, is accounted for via misalignment of the valence-band edges. The energy of the bulk valence-band edge, E_v, which is an input parameter in the EBOM, has different values on the inside ($E_v = 0$) and outside ($E_v = V_h$) of the dot boundary.

The SOBO's in Eqs.(5)–(10) could now, in principle, be used as basis functions in a variational calculation, but by exploiting the symmetry further a large reduction of the size of the computation can be achieved. Following the scheme in Ref. 17 we expand the hole wave function in a set of angular functions multiplied with radial functions. With cubic symmetry the hole ground state is fourfold degenerate (Γ_8) and the four degenerate states are decoupled and can be treated independently. In our notation these states correspond to two Γ_6 states (heavy-hole) and two Γ_7 (light-hole) states. Since it does not matter which one of the degenerate states we focus on, we arbitrarily choose to focus on $\Gamma_6^{\frac{1}{2}}$ hole states. The appropriate angular functions to use are[19]

$$|\psi_{\frac{1}{2}}^{\Gamma_6}(\mathbf{R}) >_a = |\mathbf{R}, u_{\frac{1}{2}}^{\Gamma_6} > ,$$

$$|\psi_{\frac{1}{2}}^{\Gamma_6}(\mathbf{R}) >_b = (Z^2 - \frac{1}{2}(X^2 + Y^2))/R^2 |\mathbf{R}, u_{\frac{1}{2}}^{\Gamma_6} > ,$$

$$|\psi_{\frac{1}{2}}^{\Gamma_6}(\mathbf{R}) >_c = \frac{\sqrt{3}}{2}(X^2 - Y^2)/R^2 |\mathbf{R},^1 u_{\frac{1}{2}}^{\Gamma_7} > ,$$

$$|\psi_{\frac{1}{2}}^{\Gamma_6}(\mathbf{R}) >_d = -iXY/R^2 |\mathbf{R},^1 u_{\frac{1}{2}}^{\Gamma_7} > ,$$

$$|\psi_{\frac{1}{2}}^{\Gamma_6}(\mathbf{R}) >_e = \frac{1}{\sqrt{2}}(iYZ - XZ)/R^2 |\mathbf{R},^1 u_{-\frac{1}{2}}^{\Gamma_7} > , \tag{14}$$

$$|\psi_{\frac{1}{2}}^{\Gamma_6}(\mathbf{R}) >_f = \frac{1}{\sqrt{2}}(iYZ + XZ)/R^2 |\mathbf{R}, u_{-\frac{1}{2}}^{\Gamma_6} > ,$$

$$|\psi_{\frac{1}{2}}^{\Gamma_6}(\mathbf{R}) >_g = \frac{\sqrt{3}}{2}(X^2 - Y^2)/R^2 |\mathbf{R},^2 u_{\frac{1}{2}}^{\Gamma_7} > ,$$

$$|\psi_{\frac{1}{2}}^{\Gamma_6}(\mathbf{R}) >_h = -iXY/R^2 |\mathbf{R},^2 u_{\frac{1}{2}}^{\Gamma_7} > ,$$

$$|\psi_{\frac{1}{2}}^{\Gamma_6}(\mathbf{R}) >_i = \frac{1}{\sqrt{2}}(iYZ - XZ)/R^2 |\mathbf{R},^2 u_{-\frac{1}{2}}^{\Gamma_7} > .$$

Here X, Y, and Z are the components of $\mathbf{R}$, and $R^2 = |\mathbf{R}|^2 = X^2 + Y^2 + Z^2$. A spherical cluster of sites in the fcc lattice is used in the calculations. The angular functions are combined with radial exponentials to give basis functions of the form

$$|\psi_i^{\Gamma_6}> = \sum_{\mathbf{R}} \cos\left(\frac{\pi}{2}\frac{\sqrt{X^2+Y^2+Z^2}}{R_{\text{clu}}}\right)$$
$$\times\, e^{-\alpha_i\sqrt{X^2+Y^2+\mu_i Z^2}}|\psi_{\frac{1}{2}}^{\Gamma_6}(\mathbf{R})>_{l_i}, \quad (15)$$

where R_{clu} is the radius of the spherical cluster. R_{clu} is either equal to (in the hard-wall case) or larger than the quantum-dot radius R. The origin is chosen to be at the center of the quantum dot. The cosine factor is included to tame an artificial discontinuity at the cluster boundary. The sum over $\mathbf{R}$ in (15) does not include the central site $(0,0,0)$, and the bond orbital at $(0,0,0)$ (with the right symmetry) is included separately in the basis.[20] Up to seven appropriately chosen α's, which correspond to 64 basis functions, are used in the calculations. The anisotropy parameters μ_i are all set to unity except for the smallest quantum dots with hard walls where other choices lower the energy slightly.

The radius of the spherical quantum dot is defined by[21]

$$R = \left(\frac{3N}{16\pi}\right)^{\frac{1}{3}} a, \quad (16)$$

where N is the number of sites in the quantum dot.

The electron is described within the spherical effective-mass approximation, i.e.,

$$H_e = -\frac{\hbar^2}{2m_e}\nabla_e^2 + V_{\text{QD}}(\mathbf{r}), \quad (17)$$

where m_e is the electron spherical effective mass and

$$V_{QD}(\mathbf{r}) = \begin{cases} 0 & \text{for } |\mathbf{r}| < R \\ V_e & \text{for } |\mathbf{r}| \geq R \end{cases} \quad (18)$$

is the dot potential. A set of Gaussians is used as basis functions for the electron,[22] i.e.,

$$\psi_e^i(\mathbf{r}) = e^{-\beta_i r^2}. \quad (19)$$

The matrix elements of H_e, i.e., $< \psi_e^i|H_e|\psi_e^j >$, and overlaps ($< \psi_e^i|\psi_e^j >$) are easily evaluated analytically. Seven appropriately chosen β's are used in the calculations.

The electron-hole interaction is assumed to be of the usual Coulomb form, i.e.,

$$v(|\mathbf{r}_h - \mathbf{r}_e|) = -\frac{e^2}{\epsilon|\mathbf{r}_h - \mathbf{r}_e|}. \quad (20)$$

The incorporation of this interaction in the calculational scheme is described in detail in Ref. 17.

As for the Luttinger parameters, we use in the barrier the bulk values for the well material for both the electron effective-mass m_e and the dielectric constant ϵ.

III. HOLES IN ZnS CRYSTALLITES

In this section we calculate energies of single holes in ZnS spherical quantum dots assuming an infinite barrier potential. The EBOM results are compared with results from the simple single-band effective-mass approximation and with results from the tight-binding calculations of Lippens and Lannoo.[4] In EBOM the infinite barrier potential is imposed by forcing the wave function to be zero at, and outside, the boundary of the quantum dot.

The Luttinger parameters are taken from Lawaetz,[23]

$$\gamma_1 = 2.54, \ \gamma_2 = 0.75, \ \gamma_3 = 1.09, \quad (21)$$

the lattice constant a is set to 5.41 Å[4], and for the spin-orbit splitting we use $\Delta = 70$ meV.[24] To compare with the single-band effective mass approximation we need an "equivalent" spherical effective mass m_h. It has been suggested[4] that the so-called density-of-states heavy-hole mass[23]

$$m_{\text{hd}} = m_0(\gamma_1 - \gamma_m)^{-1}(1 + 0.05\gamma_h + 0.0164\gamma_h^2)^{2/3}, \quad (22)$$

where

$$\gamma_m = (2\gamma_2^2 + 2\gamma_3^2)^{1/2},$$
$$\gamma_h = 6(\gamma_3^2 - \gamma_2^2)/[\gamma_m(\gamma_1 - \gamma_m)], \quad (23)$$

should be used. For the present Luttinger parameters one finds a density-of-states heavy-hole mass of $1.78m_0$ which turns out to be completely inadequate when comparing with our EBOM results. A much better choice is $m_h = 0.61m_0$ deduced from the tight-binding calculation of Lippens and Lannoo.[4] The single-band effective-mass expression for the ground-state energy of a hole confined in a spherical quantum dot with hard walls is[25]

$$E_h = \frac{\hbar^2\pi^2}{2m_h R^2}. \quad (24)$$

In Fig. 1 we compare the EBOM, the single-band effective-mass approximation [formula (24) with $m_h = 0.61m_0$], and the tight-binding results of Lippens and Lannoo. The EBOM results are given for a selected set of dot radii. A simple interpolation would not give a smooth curve for the smallest sizes. This is mainly due to the different surface geometries of the different clusters. Generally, a good agreement between the EBOM results and the effective-mass results with $m_h = 0.61m_0$ is observed. For the smallest clusters, however, the EBOM predicts a smaller confinement energy. The tight-binding results show an oscillatory behavior with changing dot radius. This is explained in terms of qualitative differences between clusters where the group of outmost atoms are cations and anions, respectively.[4] (In EBOM the smallest unit is a "molecule" consisting of an anion and a cation, and this oscillation is absent.) The hole confinement energy predicted by the tight-binding scheme is always lower than the EBOM value. This discrepancy presumably reflects the different bulk valence-band structures inherent in the two methods[4] (see also Sec. IV).
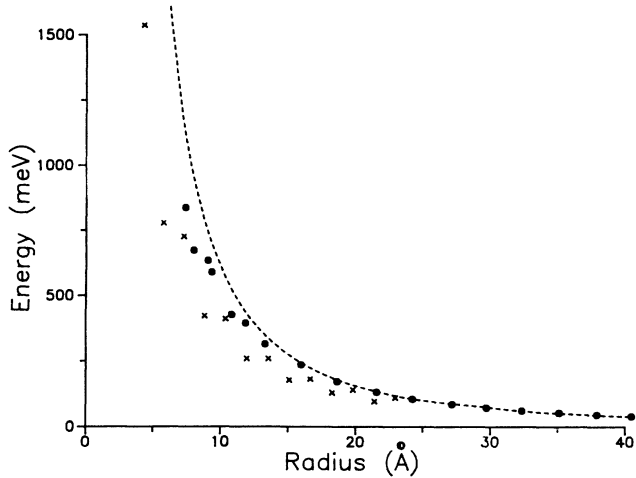
FIG. 1. Calculated ground-state energies of holes in spherical ZnS quantum dots with infinite barrier heights. The filled circles are our results obtained with EBOM, the crosses refer to the tight-binding results of Lippens and Lannoo (Ref. 4), and the dotted curve corresponds to the spherical effective-mass approximation [formula (24) with $m_h = 0.61m_0$].

The fact that the single-band effective-mass approximation with an appropriately chosen spherical hole mass m_h gives good results for the infinite-barrier-height case is not surprising. With infinite barrier heights it follows as a general result for multiband effective-mass theory that for the single-hole energy,[16,26]

$$E = cR^{-2} \tag{25}$$

as in single-band effective-mass theory (24). EBOM and multiband effective-mass theory are expected to give similar results for large quantum dot radii where the graininess of EBOM is relatively less important. Good agreement with EBOM (and multiband effective-mass theory) is thus obtained if the spherical hole mass m_h is fitted to give the right coefficent c in (25). This value of m_h is generally *not* applicable to other problems like, e.g., quantum dots with finite barrier heights where the complicated valence-band structure must explicitly be accounted for in the calculational scheme.

To check the accuracy of our calculational scheme, we compared our present results with the basis functions given in Sec. III with *exact* results (within EBOM) for clusters with radii up to 22 Å. The exact results were obtained by diagonalizing the hole Hamiltonian exactly using up to 500 symmetry-adapted shell functions as described in Ref. 27. Typically the error with the present variational scheme was found to be around 10 meV.

In Fig. 2 we show the EBOM results for the hole ground-state energy for different values of the spin-orbit splitting Δ ($\Delta = 0, \Delta = 70$ meV, $\Delta = \infty$). This figure demonstrates that the ground-state energy is not very sensitive to the value of Δ. Furthermore, the realistic value $\Delta = 70$ meV is closer to the results for $\Delta = 0$ than $\Delta = \infty$ when the confinement energy is large. This indicates that it is the *ratio* between Δ and the confinement energy which determines the importance of including the split-off band in the calculation.

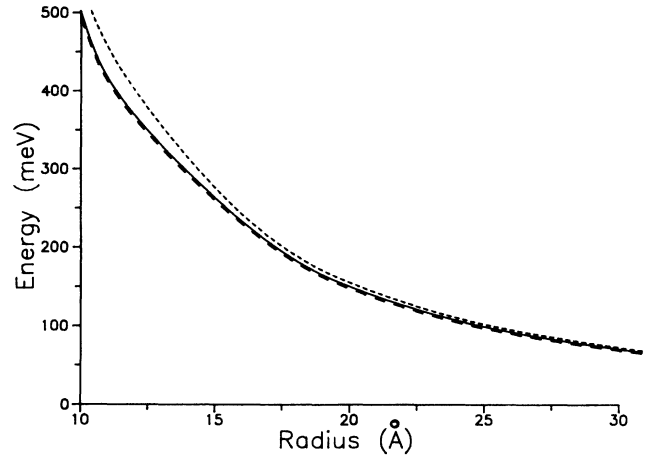FIG. 2. Calculated ground-state energies of holes in spherical ZnS quantum dots with infinite barrier heights for different spin-orbit splittings Δ. The solid curve corresponds to $\Delta = 70$ meV, the dashed curve to $\Delta = 0$, and the dotted curve to $\Delta = \infty$.

IV. EXCITONS

We now go on to calculate exciton energies in CdS crystallites for which several experimental studies have been reported.[2,6,11] Ekimov, Efros, and Onushchenko[2] have measured the confinement energy for a set of small CdS crystallites embedded in glass material. These measured high-energy shifts are smaller than predicted by (single-band) effective-mass theories assuming hard walls at the dot boundary, and finite barrier heights must be incorporated in the model to account for the experimental data.[8] This finding has been confirmed by a later experimental study of Wang and Herron[6] who used a set of different techniques to fabricate CdS crystallites with diameters between 10 and 60 Å. Even though neither the shape and surface structure of these crystallites nor the properties of the surrounding medium are well known, we believe that insight can be gained with our model.

For the CdS material parameters we adopt $a = 5.82$ Å, $m_e = 0.18m_0$ (Ref. 4) and $\epsilon = 5.5$.[6] Since bulk CdS most often is found with hexagonal structure, Luttinger parameters for CdS with zinc-blende structure are apparently not available. Lippens and Lannoo estimated the appropriate spherical effective mass for the hole to be $m_h = 0.53m_0$ based on their tight-binding calculation. In Ref. 23 the *ratios* between the Luttinger parameters for Zn- and Cd-based semiconductors are observed to be similar. We expect the appropriate value for the spherical effective mass to be roughly inversely proportional to the Luttinger parameters,[28] and thus adopt for CdS the Luttinger parameters of ZnS in Eq. (21) multiplied with the ratio between the values of the spherical hole masses in Lippens and Lannoo, i.e., $m_h(\text{ZnS})/m_h(\text{CdS})=0.61/0.53$. The Luttinger parameters used for CdS are thus

$$\gamma_1 = 2.92, \quad \gamma_2 = 0.86, \quad \gamma_3 = 1.25 . \tag{26}$$

A value for the spin-orbit splitting Δ is apparently not available either. However, since different semiconductors with common anions seem to have similar values of Δ,[24]

we apply the ZnS value, namely, $\Delta = 70$ meV, to cubic CdS as well. Since the results are not very sensitive to the value of Δ, a possible error here should have small effects on the results.

With the values given above for m_e, m_h, and ϵ we find the effective Bohr radius $a^* = (0.529 \text{ Å})\epsilon m_0(m_e^{-1} + m_h^{-1})$ to be 22 Å. In the calculation we restrict ourselves to crystallites with radii less than 40 Å. Thus $R < 2a^*$ for all cases considered, and Kayanuma's criterion for being in the strong-confinement regime is fulfilled.

In Fig. 3 we show, with solid lines, the exciton confinement energy for a set of different barrier heights. The curves are obtained by interpolating results for a discrete set of quantum dot radii. As in Ref. 8 the confining potentials are assumed to be equal for electron and hole (although justification for this choice is lacking). The uppermost solid curve corresponds to infinite barrier heights. In this case the electron basis functions (19) do not fulfill the hard-wall boundary conditions $[\psi_e(R) = 0]$, and we use the barrier height which gives, for our set of Gaussian basis functions, the correct single-electron ground-state energy in the hard-wall case [Eq.(24) with m_e instead of m_h]. In all cases considered this (artificial) barrier is much larger than any realistic barriers.

To compare with experimental data for CdS crystallites in silicate glass[2] we plot the exciton energy for $V_e = V_h = 2250$ meV. This value corresponds to an en-
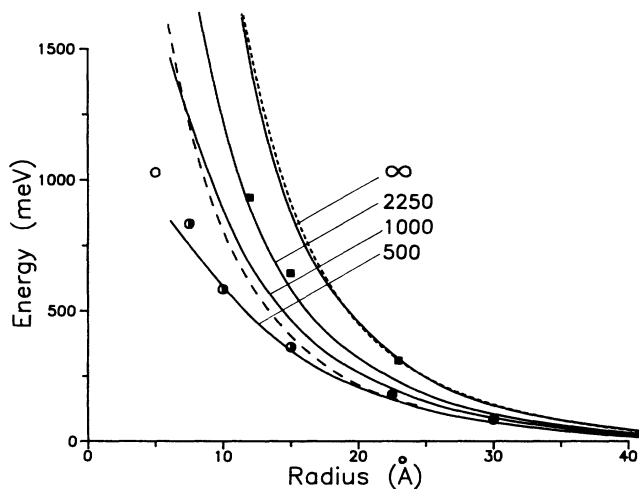

FIG. 3. Ground-state energies of excitons in CdS quantum dots. The solid curves correspond to results within our combined EBOM and effective-mass scheme. The confining potentials for the hole and electron are set equal, i.e., $V_e = V_h$. Results for infinite barrier heights (marked with ∞), $V_e = V_h = 2250$ meV, $V_e = V_h = 1000$ meV, and $V_e = V_h = 500$ meV are shown. The dashed curve represents the tight-binding results of Lippens and Lannoo (Ref. 4) (which correspond to infinite barrier heights). The dotted curve shows the results from Kayanuma's formula (1). The experimental data of Ekimov, Efros, and Onuschenko (Ref. 2) (marked with filled squares) and of Wang and Herron (Ref. 6) (circles) are indicated. Results marked with filled, half-filled, and unfilled circles correspond to quantum dots fabricated with different techniques.

ergy gap of ~ 7 eV in the barrier which has been roughly estimated for silicate glasses.[8,29] The experimental data are marked with filled squares. A good agreement between theory and experiment is observed, especially for the two smallest crystallites, and this indicates that the present incorporation of finite barrier heights is essential.

The experimental data of Wang and Herron,[6] marked with circles, correspond to lower barrier heights. Note that there is uncertainty connected to the experimental values for the crystallite radii due to size dispersion ($\sim 20\%$) of the crystallites in the sample.[6] The crystallites are embedded in organic materials, not in glass.[6] It is thus expected that the appropriate values for V_e and V_h will differ from the glass values. The curve corresponding to $V_e = V_h = 500$ meV fits the experimental data well. Note, however, that the crystallites in this experimental study were fabricated differently. The two largest crystallites (marked with filled circles) were produced with one technique, the intermediate-sized crystallites (half-filled circles) with another, and the smallest crystallite (open circle) with a third. The smallest crystallite was believed to have a pyramidal shape, and the "radius" refers to half the distance from the base to the top.[6] It is thus not certain that the appropriate values for V_e and V_h are the same in these three cases.

In Fig. 3 we also show results obtained by the tight-binding scheme of Lippens and Lannoo. This curve, which corresponds to infinite barrier heights, is found by adding the second and third term in Eq.(1), due to the electron-hole interaction, to their calculated single-particle energies. The oscillatory behavior of the single-particle energies, seen explicitly for holes in ZnS in Fig. 1, is smoothed out. The curve lies significantly lower than our infinite-barrier-height curve. Since both the EBOM and the effective-mass approximation assume dispersion relations which lie above the realistic dispersion relation, the exciton energies predicted by us are expected to be too high. This effect is most important for small quantum dots with high barriers, for which the wave function is most strongly localized and contain components with large wave vector k. On the other hand the tight-binding scheme of Lippens and Lannoo underestimates the energies of the first conduction band and is thus expected to predict too small exciton energies.[4]

The experimental data by Ekimov, Efros, and Onushchenko[2] for CdS crystallites in glass seem to favor our results compared to the tight-binding results. The experiments by Wang and Herron[6] may indicate that the tight-binding results are better, but may alternatively be accounted for in our model by assuming finite barrier heights. However, for the smallest crystallites where details in the surface become very important and where the wave function penetrates significantly into the surrounding medium, both calculational schemes may be inadequate.

In our calculation we have, with no justification, assumed $V_e = V_h$. If a different ratio between the valence-band and conduction-band offset is used, the predicted exciton energies will be different. Since the electron is lighter than the hole, a larger fraction of conduction-band offset will generally increase the confinement energy and

thus the exciton energy, and vice versa.

The dotted line in Fig. 3 corresponds to Kayanuma's limiting formula (1), based on single-band effective-mass descriptions of both hole and electron and on the assumption of infinite barrier heights. When comparing with our results (for infinite barrier heights), good agreement is observed. The difference between the exciton energy and the sum of the single-particle energies is commonly called the *binding energy*. The binding energy as a function of dot radius is plotted in Fig. 4 for the same set of barrier heights as in Fig. 3. In our combined EBOM and effective-mass scheme the binding energy is found by subtracting the exciton energy from the sum of the single-electron and single-hole energies. For comparison we also show results from Kayanuma's formula for the binding energy in the infinite-barrier-height case [absolute value of the second and third term in (1)]. A good agreement with our infinite-barrier-height results is observed also here, and this indicates that Kayanuma's expression for the binding energy is valid also when the bulk valence-band degeneracy is accounted for. As expected, the binding energy is found to decrease with decreasing barrier heights. This is due to increased penetration of the wave function into the barrier with a resulting smaller Coulomb attraction.[30] In the zero-radius and infinite-radius limit the binding energy approaches the bulk binding energy for excitons in the barrier and well materials, respectively. In the single-band effective-mass approximation the bulk binding energy is identical to the
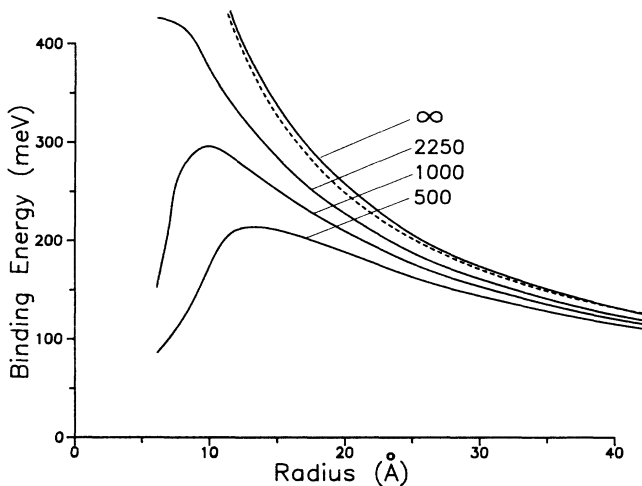

FIG. 4. Binding energies of excitons in CdS quantum dots. The solid curves correspond to results from our combined EBOM and effective-mass scheme. The confining potentials for the hole and electron are set equal, i.e., $V_e = V_h$. Results for infinite barrier heights (marked with ∞), $V_e = V_h = 2250$ meV, $V_e = V_h = 1000$ meV, and $V_e = V_h = 500$ meV are shown. The dotted curve shows the binding energy according to Kayanuma's formula [absolute value of last two terms in (1)]. For zero and infinite dot radii, the exciton binding energies correspond to the bulk values in the barrier and well materials, respectively. In the single-band effective-mass approximation the bulk binding energy [Eq.(2)] is 60 meV with our choices for the material parameters (both in the well and barrier materials).
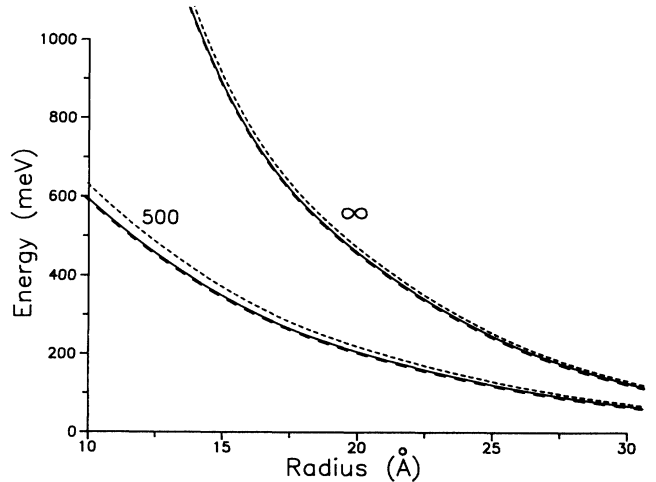

FIG. 5. Calculated exciton energies in spherical CdS quantum dots with $V_e = V_h = 500$ meV and infinite barrier heights, respectively, for different spin-orbit splittings Δ. The solid curves correspond to $\Delta = 70$ meV, the dashed curves to $\Delta = 0$, and the dotted curves to $\Delta = \infty$.

effective Rydberg energy in Eq.(2) which with our choice of material parameters is ~ 60 meV (in both the well and barrier material). Although our calculational scheme is different, 60 meV is probably a reasonable estimate for the bulk exciton binding energy in our model also. For dot radii in between the binding energy is larger, and the curve thus exhibits a maximum for a finite dot radius. The same feature has previously been seen for the impurity binding energies in quantum dots.[27,31]

In Fig. 5 we show the sensitivity of the exciton energy to the value of the spin-orbit splitting Δ for $V_e = V_h = 500$ meV and for infinite barrier heights, respectively. Although small, the difference between the $\Delta = 0$ and $\Delta = \infty$ results are slightly larger than for the single-hole results in Fig. 2.

Experimental observations on ZnS crystallites have also been reported. For 10-Å crystallites in methanol solution, a high-energy shift of 0.7 eV was observed.[11] Lippens and Lannoo predicted a shift of 0.3 eV in their tight-binding scheme. With $m_e = 0.42 m_0$ (Ref. 4) and $\epsilon = 5.2$ (Refs. 4 and 11) [and the Luttinger parameters (21)] we find 0.87 eV assuming infinite barrier heights, in better agreement with the experimental value. Finite barrier heights will further reduce the predicted exciton energy and may improve agreement with experiment.

V. CONCLUDING REMARKS

We have calculated single-hole energies in ZnS crystallites and bound-exciton energies in CdS and ZnS crystallites using a combined EBOM and effective-mass approach. The calculational scheme is superior to previous schemes in that it includes the complicated valence-band structure in bulk, finite barrier heights, and the electron-hole interaction *simultaneously*. With reasonable choices of input parameters, available experimental data can be accounted for, but more accurate and certain parameter

values are needed to get conclusive answers.

The three methods which have been used so far in the description of excitons in crystallites, namely, the effective-mass approximation, the EBOM, and the empirical tight-binding method[4] have in common that the input parameters are determined from bulk band structure. This is an uncertain approximation for the smallest clusters. Based on the inherent band structures of the different methods it is expected that the effective-mass approximation and the EBOM overestimates confinement energies while the tight-binding method underestimates them. In particular, the application of the bulk value of the spin-orbit splitting Δ is uncertain. However, our study shows that the results are not very sensitive to this parameter. More advanced calculations are encouraged for small clusters to possibly clarify the situation and to estimate the validity and limitations of the above-mentioned methods.

*Present address: Department of Physics, University of California San Diego, LaJolla, CA 92093.

[1] L.E. Brus, J. Chem. Phys. 79, 5566 (1983); ibid. 80, 4403 (1984).

[2] A.I. Ekimov, Al.L. Efros, and A.A. Onushchenko, Solid State Commun. 56, 921 (1985).

[3] Y. Kayanuma, Phys. Rev. B 38, 9797 (1988).

[4] P.E. Lippens and M. Lannoo, ibid. 39, 10 935 (1989).

[5] P.E. Lippens and M. Lannoo, Phys. Rev. B 41, 6079 (1990).

[6] Y. Wang and N. Herron, Phys. Rev. B 42, 7253 (1990).

[7] Y. Wang and N. Herron, J. Phys. Chem. 95, 525 (1991).

[8] Y. Kayanuma and H. Momiji, Phys. Rev. B 41, 10 261 (1990).

[9] See references listed in Y. Kayanuma, Phys. Rev. B 38, 9797 (1988); P. E. Lippens and M. Lannoo, ibid. 39, 10 935 (1989).

[10] R. Rossetti, J.L. Ellison, J.M. Gibson, and L.E. Brus, J. Chem. Phys. 80, 4464 (1984).

[11] R. Rossetti, R. Hull, J.M. Gibson, and L.E. Brus, J. Chem. Phys. 82, 552 (1985).

[12] S.V. Nair, S. Sinha, and K.C. Rustagi, Phys. Rev. B 35, 4098 (1987).

[13] C.F. Lo and R. Sollie, Solid State Commun. 75, 775 (1991).

[14] Y.-C. Chang, Phys. Rev. B 37, 8215 (1988).

[15] J.M. Luttinger, Phys. Rev. 4, 1030 (1956).

[16] J.M. Luttinger and W. Kohn, Phys. Rev. 97, 869 (1955).

[17] G.T. Einevoll, D.S. Citrin, and Y.-C. Chang, Phys. Rev. B 44, 8068 (1991).

[18] A Kane-like model [E.O. Kane, J. Phys. Chem. Solid 1, 249 (1957)] which couples the electron and hole explicitly is not necessary for large-gap materials.

[19] G.T. Einevoll and Y.-C. Chang, Phys. Rev. B 41, 1447 (1990).

[20] This is for "historical" reasons. In the application to isoelectronic impurities in Ref. 17 this separation is useful. Here it does not matter.

[21] This is analogous to the definition of the radius in the tight-binding calculation of Lippens and Lannoo (Ref. 4).

[22] Since we are in the strong-confinement regime, the electron wave function is expected to resemble the ground-state wave function of the single-electron problem. Contributions from higher-order spherical harmonics (e.g., d-like) are thus expected to be negligible.

[23] P. Lawaetz, Phys. Rev. B 4, 3460 (1971).

[24] J. Bernholc and S. Pantelides, Phys. Rev. B 15, 4935 (1977).

[25] See, for example, S. Gasiorowicz, Quantum Physics (Wiley, New York, 1974).

[26] P.C. Sercel and K.J. Vahala, Phys. Rev. B 42, 3690 (1990).

[27] G.T. Einevoll and Y.-C. Chang, Phys. Rev. B 40, 9683 (1989).

[28] This applies, for example, to light-hole and heavy-hole masses perpendicular to the growth direction in quantum wells. [See, e.g, p.141 in G. Bastard, Wave Mechanics Applied to Semiconductor Heterostructures, Les Editions de Physique (Les Ulis, France, 1988.)] Also, for small values of γ_h, this is nearly fulfilled for the density-of-state heavy-hole mass in (22) and (23).

[29] A.N. Trukhin, M.N. Tolstoi, L.B. Glebov, and V.L. Savelev, Phys. Status Solidi 99, 155 (1980).

[30] According to (1) the effects of the Coulomb attraction grow in the hard-wall case as $1/R$, where R is the dot radius and thus also a measure of the spatial extension of the wave functions. In the more general case we thus expect that larger spatial extensions of the wave functions will reduce the effect of the Coulomb attraction and consequently the binding energy.

[31] J.-L. Zhu, Phys. Rev. B 39, 8780 (1989).